*Graphical Abstract

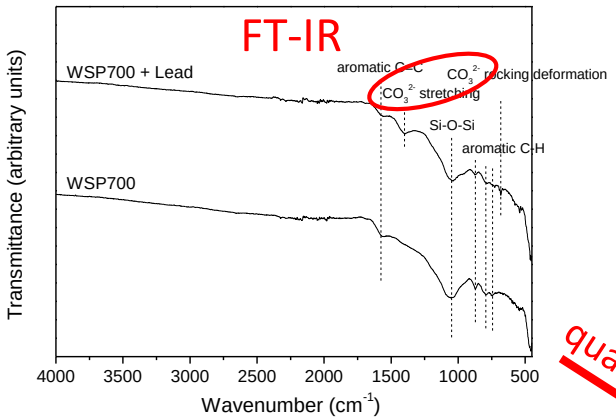

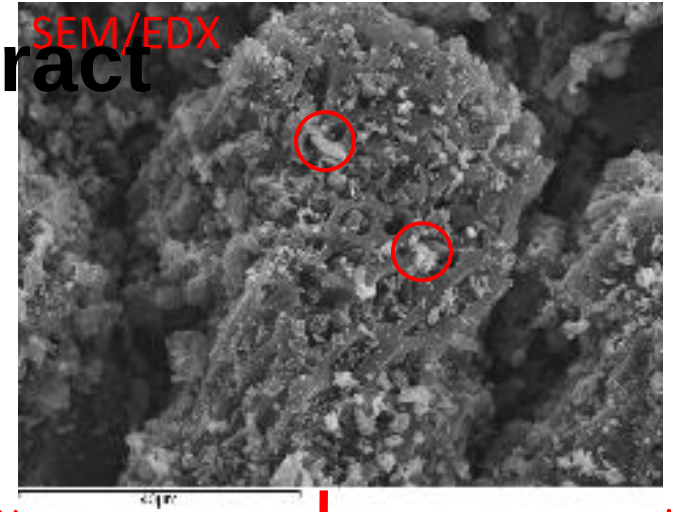

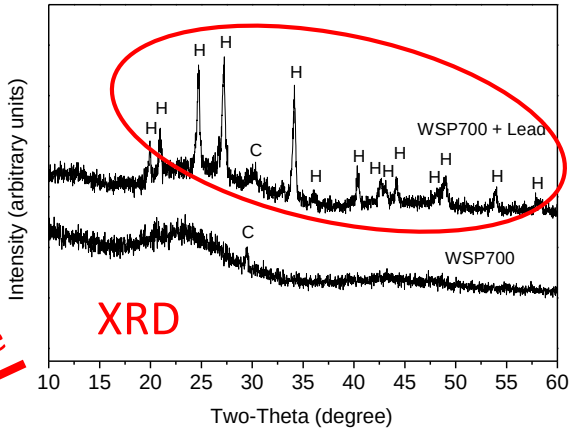

qualitative

qualitative

qualitative

Adsorbed Pb^{2+} on biochar

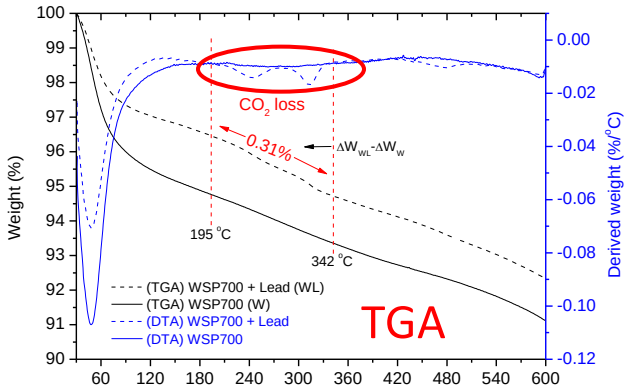

quantitative

quantitative

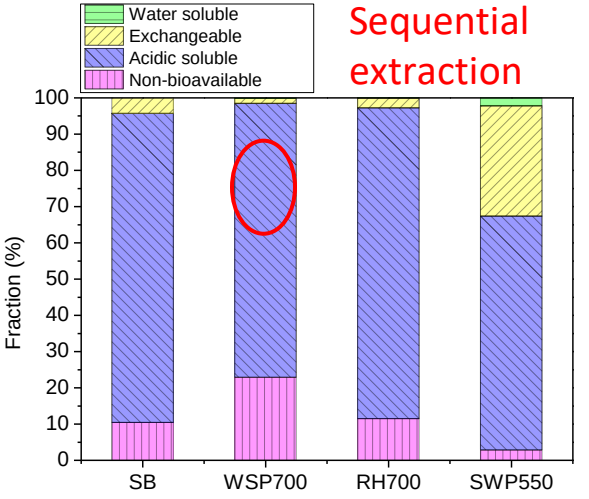

Characterise the adsorption mechanisms of Pb^{2+} on biochar

***Highlights (for review)**

- Pb^{2+} mainly exists as acid soluble fraction (75.61-85.76%) on SB, WSP700 and RH700
- 82.24% of total adsorbed Pb^{2+} exists as cerussite on SB
- 13.00-29.70% of total adsorbed Pb^{2+} exists as hydrocerussite on rest three biochars
- The rest acidic soluble fraction for Pb^{2+} is likely adsorbed through cation-π interaction
- Using chemical and micro-structural methods to quantify mechanisms is feasible

Qualitative and quantitative characterisation of adsorption mechanisms of lead on four biochars

Zhengtao Shen[a,b,*], Yiyun Zhang[a], Fei Jin[a], Oliver McMillan[a], Abir Al-Tabbaa[a]

[a](Geotechnical and Environmental Research Group, Department of Engineering, University of Cambridge, Cambridge, CB2 1PZ, United Kingdom)

[b](Department of Earth and Atmospheric Sciences, University of Alberta, Edmonton, T6G 2E3, Canada)

*Corresponding author: Email: ztshennju@gmail.com; zs281@cam.ac.uk. Phone number: 0044+7541935253. Fax: 0044+7541935253

Abstract: The adsorption mechanisms of lead (Pb^{2+}) on four biochars (SB produced from British hardwood at 600 °C and three standard biochars produced from wheat straw pellets at 700 °C (WSP700), rice husk at 700 °C (RH700) and soft wood pellets at 550 °C (SWP550)) were characterised qualitatively and quantitatively, using a combination of chemical and micro-structural methods. Sequential extraction test results show that Pb^{2+} was predominantly adsorbed on SB (85.31%), WSP700 (75.61%) and RH700 (85.76%) as acidic soluble fraction, which was potentially bioavailable if applied in soil. The exchangeable fraction for SB, WSP700 and RH700 was low (1.38-4.29%) and their water soluble fraction was negligible (0-0.14%). Micro-structural analysis further investigated this fraction and confirmed the presence of cerussite ($PbCO_3$) on SB and hydrocerussite ($Pb_3(CO_3)_2(OH)_2$) on WSP700, RH 700 and SWP550, suggesting a mechanism of surface precipitation for Pb^{2+} adsorption on the biochars. The percentages of Pb^{2+} in the form of $PbCO_3$ on SB (82.24%) and $Pb_3(CO_3)_2(OH)_2$ on WSP700 (13.00%), RH 700 (19.19%) and SWP550 (29.70%) were quantified using thermogravimetric analysis (TGA). This study suggests that it is feasible to quantify different adsorption mechanisms of Pb^{2+} on biochars, which is important for the practical application of biochar in water and/or soil treatment.

Keywords: biochar; quantitative; characterisation; adsorption mechanism; lead; speciation

45

46 1. Introduction

47 Biochar is a charcoal-like material produced from agricultural and industrial organic
48 wastes (Lehmann, 2007; Sohi, 2012). Pyrolysis is the typical production process for
49 biochar during which the feedstock (typically biomass) is carbonised and
50 subsequently biochar, bio-oil and syn-gas are produced (Jahirul et al., 2012; Sohi,
51 2012). Biochar production converts the labile biomass to a recalcitrant form
52 (Lehmann et al., 2008). When added to soil, a meta-analysis showed that 97% of
53 biochar carbon are recalcitrant and can remain in the soil for approximately 556
54 years (Wang et al., 2016).

55 Engineered biochars have demonstrated high adsorption capacities for heavy metals
56 due to their aromatic structure and high pH, surface area and cation exchange
57 capacity (CEC) (Lehmann, 2007; Sohi, 2012; Beesley et al., 2011). Biochar has
58 effectively immobilised heavy metals when applied to contaminated soil. Bian et al.
59 (2014) conducted a three-year study using wheat straw biochar to treat agricultural
60 land contaminated with Cd^{2+} (5 mg/kg) and Pb^{2+} (100 mg/kg). During the three years
61 after the treatment, Cd^{2+} and Pb^{2+} concentrations were continuously reduced in both
62 $CaCl_2$ and DTPA extractions, and in crop biomass. Shen et al. (2016b) applied a
63 hardwood biochar to a severely contaminated industrial site and observed that the
64 leachability of Ni^{2+} (from 0.35% to 0.12-0.15%) and Zn^{2+} (from 0.12% to 0.01%) was
65 significantly reduced three years after biochar treatment. Numerous studies have
66 also shown biochar's effectiveness in water treatment (Cui et al., 2016b; Qian et al.,
67 2016; Shen et al., 2017). A recent meta-analysis study compared the life cycle
68 environmental and economic performance of biochar with activated carbon, which is

one of the most conventional adsorbents used in soil remediation (Alhashimi and Aktas, 2017). It was found that biochar has lower energy demand (6.1 MJ/kg versus 97 MJ/kg), global warming potential impact (−0.9 kg CO_2eq./kg and 6.6 kg CO_2eq./kg) and cost (5 $/kg versus 5.6 $/kg). When adsorption of heavy metals was used as the functional unit during analysis, results indicate that biochar had lower environmental impacts than activated carbon. Therefore, the use of biochar in water treatment or soil remediation to immobilise heavy metals and reduce their environmental risks is regarded as a green sustainable remediation technology due to both its effectiveness in immobilising heavy metals and its additional benefits in waste management, energy production and carbon storage (Lehmann et al., 2006).

Adsorption is the main mechanism for biochar to immobilise heavy metals in water and soil (Sizmur et al., 2015). Biochar can adsorb heavy metals through a range of mechanisms including physical adsorption, cation exchange, cation-π interaction, surface precipitation and surface complexation (Cao et al., 2009; Choy and McKay, 2005; Keiluweit et al., 2009; Mohan et al., 2007; Zhang et al., 2015). Different adsorption mechanisms have different environmental implications. The heavy metals adsorbed on biochar through physical adsorption and cation exchange represent the readily bioavailable fraction in soil which poses direct risks to plants and humans, whereas those adsorbed through cation-π interaction represent the potentially bioavailable fraction, and those through surface complexation represent the non-bioavailable fraction (Rodriguez-Vila et al., 2015). The bioavailability of heavy metals adsorbed on biochar through surface precipitation depends on precipitate type: the precipitates which can be dissolved in sodium acetate or acetic acid is regarded as potentially bioavailable and the rest is regarded as non-bioavailable. When applied to contaminated soil, it is expected that biochar could reduce the readily bioavailable

heavy metals to reduce the environmental risks. However, when applied in water treatment, the physically bonded and exchangeable heavy metals on biochar are easily desorbed, which will aid the reuse of biochar.

The adsorption mechanisms of heavy metals on biochar vary among biochars produced from different feedstocks at different temperatures due to their different properties (Choy and McKay, 2005; Keiluweit et al., 2010; Mohan et al., 2007; Zhang et al., 2015). For instance, plant feedstock contains mainly cellulose, hemicellulose and lignin however the proportion of each of the three components in different plants (e.g. grass versus wood) varies (Jahirul et al., 2012). The lignin, hemicellulose and cellulose also thermally decompose at different temperatures: hemicellulose decomposes between around 240 and 400 °C; cellulose between around 320 and 410 °C; and lignin only partially decomposes under heating up to 500 °C. The different degrees of thermal decomposition of feedstocks will result biochars with significantly different properties (e.g. pH, CEC and surface area) (Keiluweit et al., 2010) and consequently different adsorption capacities for heavy metals. Therefore, it is important to identify the adsorption mechanisms of heavy metals on biochar in order to direct its practical applications and predict its environmental performances. In addition, when applied to field contaminated land, environmental factors such as rainfall, groundwater flow, soil microbial activity, plant growth and earthworm movement may affect the long-term stability of heavy metals adsorbed by biochar. Understanding the adsorption mechanisms of heavy metals on biochar prior to field application will aid the selection of biochar, the engineering design and estimation/modelling of the resistance and long-term stability of biochar immobilisation of heavy metals on field conditions.

Batch adsorption studies are the most conventional methods to investigate the adsorption mechanisms of heavy metals on biochar. The adsorption mechanisms can be inferred through the adsorption characteristics obtained from batch adsorption studies. Micro-structural methods such as X-ray diffraction (XRD), Fourier transformed infrared (FT-IR) spectra and scanning electron microscopy (SEM) and energy dispersive X-ray (EDX) analysis are typically used with batch adsorption studies to indicate the adsorption mechanisms of heavy metals on biochar (Cheng et al., 2016; Cui et al., 2016a; DeMessie et al., 2015). The minerals formed, the change of the molecular structure and the surface morphology of biochar after heavy metal adsorption can be used to indicate the adsorption mechanisms. However, these micro-structural analyses remain at a qualitative level, with very limited investigations quantifying the fractions of heavy metals adsorbed on biochar through different mechanisms being published to date. Xu et al. (2014) quantified the portions of different precipitates on a manure and a rice straw biochar after Pb^{2+} adsorption using MINTEQ modelling (accompanied with adsorption studies, XRD and FT-IR tests) (Xu et al., 2014). They found that 91.6% and 67.5% of the total adsorbed Pb^{2+} on the inorganic part of the two biochars can be attributed to precipitation, and subsequently quantified the portions of different precipitates ($Pb_5(PO_4)_3Cl$ and $Pb_3(CO_3)_2(OH)_2$). However, experimental results are needed to verify these findings obtained through MINTEQ modelling. Fristak et al. (2015) used a chemical method called sequential extraction combined with adsorption studies and FT-IR analysis to investigate the adsorption mechanisms of Cd^{2+} to two woody biochars and an activated carbon both qualitatively and quantitatively (Fristak et al., 2015). They found 69-92% of the adsorbed Cd^{2+} existed in the exchangeable and acidic soluble fractions. However, this study did not quantitatively separate the exchangeable and

143 acidic soluble fractions of Cd^{2+} on biochars which pose different environmental risks.
144 The quantification of the adsorption mechanisms of heavy metals on biochar needs
145 further understanding.

146 It is therefore important to characterise the adsorption mechanisms of heavy metals
147 on biochar both qualitatively and quantitatively to aid its practical application. Pb^{2+}
148 was selected as the target metal in this study as it is among the most serious
149 concerns for water and soil pollution (Yang et al., 2014) and all the four biochars
150 exhibited the highest adsorption capacities for Pb^{2+} compared with other heavy
151 metals. Previous studies about biochar adsorption of Pb^{2+} mainly investigated the
152 adsorption characteristics through batch adsorption tests (Liu and Zhang, 2009;
153 Mohan et al., 2007; Qiu et al., 2008). Several mechanistic investigations on Pb^{2+}
154 adsorption on biochar remain at a qualitative level (Cao et al., 2009; Inyang et al.,
155 2011). In this study, A modified sequential extraction test was used to quantify
156 different speciation of Pb^{2+} on biochar, which represents different environmental
157 risks. Thermogravimetric analysis (TGA) was used to quantify the thermally
158 decomposable minerals (Pb^{2+} precipitates) formed on biochar after Pb^{2+} adsorption.
159 XRD, FT-IR and SEM/EDX were used to qualitatively investigate the adsorption
160 mechanisms of lead (Pb^{2+}) on biochars. XRD and SEM/EDX were expected to
161 identify the potential formation of Pb^{2+} precipitates on biochars' surface. FT-IR was
162 expected to identify the potential change of functional groups of biochar resulting
163 from complexation or other interactions with Pb^{2+}. This experimental study aims to
164 investigate the adsorption mechanisms of Pb^{2+} on biochar both qualitatively and
165 quantitatively, so as to aid the understanding of its environmental implications.

166 2. Materials and methods

2.1 Biochar

Four biochars were used in this study. Salisbury biochar (SB) was obtained from Southern Woodland Products (Salisbury, UK). It was produced from British broadleaf hardwood at a pyrolysis temperature of 600 ºC in a retort with a residence time of 13.5 h. SB was previously applied to a field contaminated site in the UK and exhibited excellent performance in immobilising Ni^{2+} and Zn^{2+} in a sandy soil throughout a three-year study (Shen et al., 2016a). In contrast, SB did not affect the mobility or speciation of Pb^{2+} in kaolin in a short-term study (Shen et al., 2016b). Therefore, SB was chosen in this study to further investigate its adsorption mechanisms for heavy metals. In previous studies, the adsorption characteristics of heavy metals on eight standard biochars were investigated. The standard biochars were produced and recommended by the UK Biochar Research Centre (UKBRC) at the University of Edinburgh (Shen et al., 2017a, 2017b). Wheat straw pellets biochar produced at 700 °C (WSP700), rice husk biochar produced at 700 °C (RH700), and soft wood pellets biochar produced at 550 °C (SWP550) were selected for this study as they exhibited a maximum, intermediate and minimum adsorption capacities for heavy metals among the eight standard biochars. The biochars were oven dried at 60 °C for 48 h and ground and sieved to a particle size smaller than 0.15 mm. The volatile matter content, total ash content and elementary contents (C, H, N, O) of SB are determined based on UKBRC standard. Other properties for SB and selected physicochemical properties of WSP700, RH700 and SWP550 can be found from the previous studies (Shen et al., 2015, 2016a, 2016b, 2017) and are also shown in Table 1.

The maximum adsorption capacities of Pb^{2+} on the biochars are shown in Table 1. The equilibrium data were calculated and fitted by the Langmuir isotherm model to

obtain the maximum adsorption capacities of Pb^{2+} for the biochars based on the methods from Shen et al. (2015). The fitting parameters and regression coefficients are shown in Fig. S1 and Table S1. The maximum adsorption capacities of Pb^{2+} on SB, WSP700, RH700 and SWP550 calculated through Langmuir fitting are 0.230, 0.549, 0.169 and 0.039 mmol/g, equal to 47.61, 113.64, 34.98 and 8.07 mg/g respectively. The equilibrium data are well described by the Langmuir model for all biochars (R^2 of 0.988-0.999).

Table 1 Physicochemical properties of the biochars (Shen et al., 2015, 2016a, 2016b, 2017).

	SB	WSP700	RH700	SWP550
BET surface area (m^2/g)	5.30	23.20	42.00	26.40
Cation exchange capacity (cmol/kg)	7.20	12.50	5.36	2.53
pH	6.96	10.03	9.81	7.91
pH_{pzc}	6.3	7.4	7.5	7.8
Volatile matter (%)	19.26	7.38	4.99	14.20
Total ash (%)	2.98	23.82	47.93	1.25
C (%)	78.92	69.04	47.32	85.52
H (%)	3.61	1.18	0.63	2.77
O (%) (by difference)	13.82	5.30	2.06	10.36
N (%)	0.67	1.32	0.85	<0.10
O/C	0.18	0.08	0.04	0.12
(O+N)/C	0.19	0.10	0.06	0.12
H/C	0.05	0.02	0.01	0.03
P (%)	N.A.	0.25	0.16	0.06
Pb (%)	0.01	bdl	bdl	bdl
Maximum Pb^{2+} adsorption capacity	0.230	0.549	0.169	0.039

	(mmol/g) (Langmuir fitting)

(N.A. – not available, bdl – below detection limit)

2.2 Chemical and micro-structural analyses

The equilibrium study revealed that all four biochars reached their maximum adsorption capacities for Pb^{2+} at initial Pb^{2+} concentration of 5 mM. Therefore, the biochar samples after Pb^{2+} adsorption at this initial solution concentration were chosen for the chemical and micro-structural tests for the greatest chance of identifying the adsorption mechanisms.

The biochar after Pb^{2+} adsorption was quickly washed using 20 mL deionised water and the water was discarded after centrifugation. A pre-trial study indicates that the influence of washing on the total amount of adsorbed Pb^{2+} was negligible. The remaining solid was oven dried at 60 °C for 48 h to represent the biochar sample after Pb^{2+} adsorption for further analysis. The same procedure was employed on the control sample without the presence of $Pb(NO_3)_2$ to represent the biochar sample before Pb^{2+} adsorption for further tests. In order to qualitatively and quantitatively characterise the adsorption mechanisms, the biochar samples before and after Pb^{2+} adsorption were examined using the following chemical and micro-structural analyses.

The 5-step sequential extraction test is typically used to indicate the speciation and bioavailability of heavy metals in soil (Li et al., 1995, 2001; Tessier et al., 1979). As sequential extraction is a time consuming test method, it is useful to simplify the test method while still efficiently determining heavy metal speciation. Since steps 3, 4 and 5 in the conventional method all represent non-bioavailable fractions of heavy metals, a simplified 4-step sequential extraction was developed in which the original

steps 3, 4 and 5 are combined. In addition, a step representing the water soluble or physically adsorbed fraction of heavy metals on biochar was added to determine their readily bioavailable fraction in soil. The two steps representing exchangeable (readily bioavailable) and acidic soluble (potentially bioavailable) fractions respectively in the 5-step procedure remained in the 4-step procedure. The Pb^{2+} in the solid residue from the equilibrium study (as detailed above) was therefore extracted and defined as the following four steps:

Step 1 – water soluble fraction: The solid residue (0.1 g biochar + adsorbed Pb^{2+}) was mixed with 20 mL deionised water and shaken for 24 h at room temperature (20 °C);

Step 2 – exchangeable fraction: The solid residue from step 1 was extracted with 8 mL of 0.5 M $MgCl_2$ (adjusted to pH 7.0 using NaOH or HCl) and shaken for 20min at room temperature;

Step 3 – acidic soluble fraction: The solid residue from Step 2 was extracted with 8 mL of 1 M NaOAc (adjusted to pH 5.0 with HOAc) and shaken for 5 h at room temperature;

Step 4 – non-bioavailable fraction: The solid residue from step 3 was digested with 9 mL of 36% HCl and 3mL of 70% HNO_3 for 16 h at room temperature and then heated at 95 °C for 2 h.

In sequential extraction, shaking in step 1, 2 and 3 was performed at 200 rpm. Following each step, the samples were centrifuged at room temperature. The supernatant was then collected and filtered through a 0.45 μm filter and acidified or diluted when necessary before analysis with ICP-OES to determine the Pb^{2+} concentration. The remaining solid sample was washed with 20 mL deionised water

prior to the next extraction step, and the washing solution was discarded after centrifugation.

XRD was used to indicate the crystalline phases in the sample. The dry samples were mounted on a flat holder and examined by a Siemens D500 X-ray diffractometer with a CuKα source operating at 40 kV and 40 mA, emitting radiation at a wavelength of 1.5405 Angstroms. The scanning regions were between 2θ values of 10-60° at a rate of 0.6 s/step and a resolution of 0.02°/step.

FT-IR was used to study the fundamental vibrations and associated rotational-vibrational structure. The infrared spectrum of biochar was tested by a Perkin Elmer Spectrum 100 Fourier transform infrared spectroscopy spectrometer. 16 scans were taken from 4000 to 450 cm^{-1} with a resolution of 4 cm^{-1}.

TGA measures the weight loss with precision while heating the biochar samples. In order to quantify the possible precipitates (e.g. cerussite and hydrocerussite) that formed after biochar adsorption of Pb^{2+}, the biochar sample was analysed using Mettler-Toledo TGA/DSC 1 Thermogravimetric Analyzer. Biochar samples of approximately 10 mg were placed into the ceramic crucible and heated from 30 to 600 °C at a heating rate of 10 °C/min under N_2 atmosphere at flow rate of 30 mL/min. The first derivatives of the TG curves (DTG) were calculated to identify the thermal decomposition of the possible precipitates.

SB was coated with gold and its surface morphology was examined by a Phenom Pro desktop Scanning electron microscopy at 5 kV. The surface morphology of the WSP700, RH700 and SWP550 were examined by a FEI Quanta 200 FEI system with an acceleration voltage of 20 kV after being coated with gold. After Pb^{2+}

adsorption, the surface morphology and elemental composition of biochars were examined by a JSM-5800LV SEM with EDX at 10 kV after being coated with Pd.

2.3. Quality control

Sequential extraction tests were performed in duplicates. All micro-structural tests were carried out once, with pre-trials being conducted to check the reproducibility. The preparation of biochar samples and sequential extraction test were conducted at a temperature controlled lab at 20 ± 1 °C and 50 ± 2% humidity. The micro-structural tests were carried out at ambient temperatures.

3. Results and discussion

3.1 Sequential extraction results

The speciation of Pb^{2+} on each biochar determined by sequential extraction tests, are shown in Fig. 1. The recovery percentages from the sequential extraction tests are shown in Table S2. The recoveries of Pb^{2+} from SB, WSP700 and RH700 were 78.41-85.52%, while that for SWP550 (46.16%) was much lower. The sequential extraction recovery of Pb^{2+} from SB, WSP700 and RH700 is similar to the recovery of heavy metals from biochar or biochar treated soils using conventional sequential extraction methods in previous studies. Fristak et al. (2015) conducted a 4-step sequential extraction test (steps 2, 3, 4 and 5 in conventional methods) on two woody biochars after adsorption of Cd^{2+}, Zn^{2+} and Cu^{2+}, and observed a recovery range of 82.4-104.4% (Fristak et al., 2015). The conventional sequential extraction recovery of Pb^{2+} from SB treated soil was 61.50-97.28% (Shen et al., 2016b). SWP550, which has the lowest recovery, also had the lowest adsorption capacity of Pb^{2+}, indicating that sequential extraction tests may not work well for samples with low adsorbed heavy metal contents due to the large relative standard errors. The

295 discussion about the sequential extraction results below will not include SWP550
296 considering its low recovery.

297 The sequential extraction results indicate that the majority of adsorbed Pb^{2+} on SB
298 (85.31%), WSP700 (75.61%) and RH700 (85.76%) were in the acidic soluble fraction.
299 WSP700 had a non-bioavailable fraction of 22.86% whereas this fraction for SB and
300 RH700 was 10.40% and 11.40% respectively. The exchangeable fraction for all the
301 three biochars was low (1.38-4.29%) and their water soluble fraction was negligible
302 (0-0.14%). The negligible water soluble fraction suggests the adsorption of Pb^{2+} to
303 the three biochars was a chemical rather than physical process (Inyang et al., 2015).
304 The low exchangeable fraction together with the negligible water soluble fraction
305 indicates an absence of the readily bioavailable fraction of Pb^{2+} on the three biochars.
306 The majority of Pb^{2+} was acidic soluble which represents a potentially bioavailable
307 fraction. This fraction may come from the formation of Pb^{2+} precipitates which can be
308 dissolved in the NaOAc/HOAc solution (step 3 in sequential extraction). Alternatively,
309 it may result from the adsorbed Pb^{2+} on biochar through cation-π interaction. Cation-
310 π interaction is a typical mechanism for biochar adsorption of heavy metals (Wang
311 et al., 2014; Keiluweit and Kleber, 2009). Unlike the weak electrostatic attraction, the
312 Pb^{2+} adsorbed through cation-π interaction has a relatively high binding energy and
313 will only desorb under significant pH changes (Wang et al., 2014; Keiluweit and
314 Kleber, 2009). Table S2 shows the change of solution pH between steps 2 and 3,
315 where the equilibrium solution pH decreased from above pH_{pzc} to below pH_{pzc}. This
316 would result in the surface charge of the biochar changing from negative to positive,
317 therefore the adsorbed Pb^{2+} through cation-π interaction would be desorbed at step
318 3 due to electrostatic repulsion (Keiluweit and Kleber, 2009). The non-bioavailable

fraction may come from the Pb^{2+} adsorbed via surface complexation or the formation of precipitates that cannot be dissolved in the NaOAc/HOAc solution.

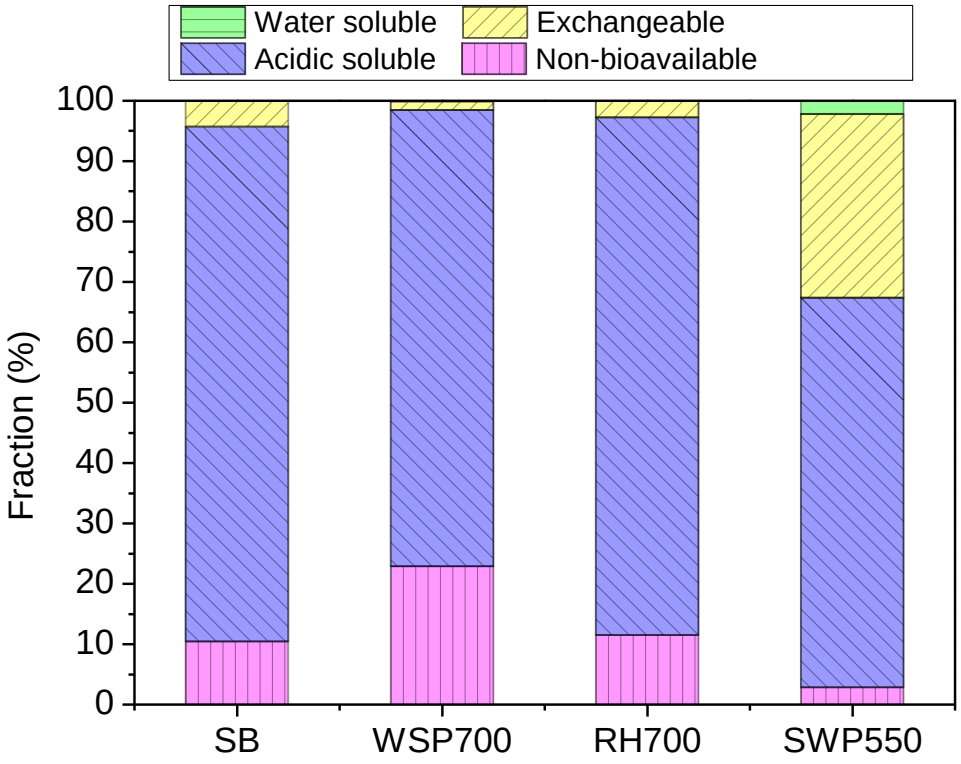

Fig. 1. Speciation of lead on biochars.

3.2 XRD and FT-IR results

It was found from the sequential extraction results that the majority of Pb^{2+} on SB, WSP700 and RH700 exists as the acidic soluble fraction, representing an adsorption mechanism of either surface precipitation or cation-π interaction. XRD and FT-IR tests were carried out to verify the formation of precipitates and changes of functional groups caused by cation-π interaction respectively.

The XRD patterns of the four biochars are shown in Fig. 2. Strong evidence was obtained from XRD patterns suggesting the formation of cerussite ($PbCO_3$) on SB, and hydrocerussite ($Pb_3(CO_3)_2(OH)_2$) on WSP700, RH 700 and SWP550. The CO_3^{2-}

that formed these precipitates could be generated from the carbonates in biochar that formed during production due to the decomposition of carboxylates (Dodson, 2011), This theory is supported by the presence of calcite ($CaCO_3$) in SB and WSP700 in the XRD patterns (Fig. 2a and 2b). The absence of peaks associated with carbonates for RH700 and SWP550 (Fig. 2c and 2d) may be due to their low concentrations. The CO_3^{2-} may also come from the dissolved CO_2 in solution from the air during adsorption tests. It was found in this study that a higher biochar pH (WSP700, RH 700 and SWP550) favoured the formation of $Pb_3(CO_3)_2(OH)_2$ while a lower biochar pH (SB) aided the formation of $PbCO_3$ in this study. A previous study observed that $Pb_3(CO_3)_2(OH)_2$ can transfer to $PbCO_3$ in the presence of a weak acid (Haizhou et al., 2008), which is in line with our finding that lower pH biochar favoured the formation of $PbCO_3$.

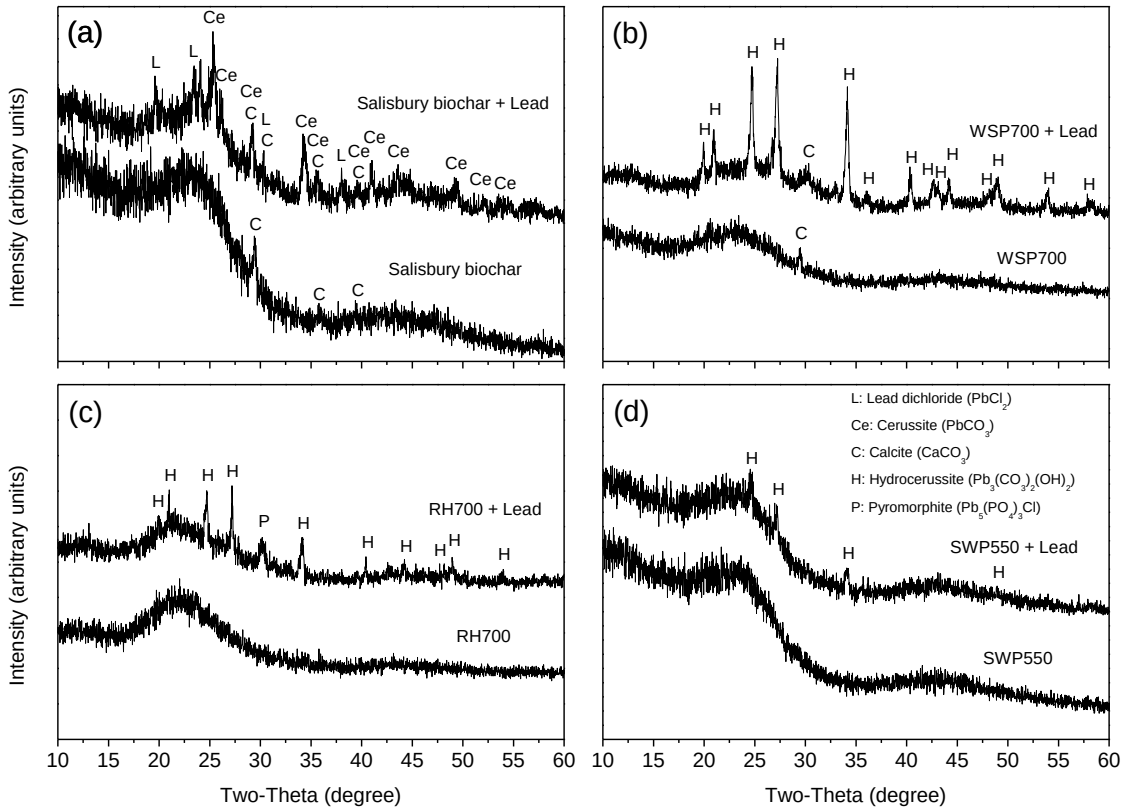

Fig. 2. XRD patterns of biochars before and after Pb^{2+} adsorption (a – Salisbury biochar (SB), b – WSP700, c – RH700, d – SWP550).

The FT-IR spectra of the four biochars are shown in Fig. 3. A new peak representing CO_3^{2-} stretching appeared on the FT-IR spectra of WSP700 after Pb^{2+} adsorption (Fig. 3a), which is likely from the $Pb_3(CO_3)_2(OH)_2$ as suggested by the XRD results. The minerals formed on SB, RH700 or SWP550 suggested by XRD patterns were not identified by FT-IR test, probably due to their lower contents. The peaks associated with aromatic C for the four biochars did not reveal significant changes after Pb^{2+} adsorption. Shifts of FT-IR peaks associated with carbonyl, hydroxyl and ester were observed for water hyacinths biochars after Cd^{2+} and Pb^{2+} adsorption in a previous study (Ding et al., 2016), suggesting an adsorption mechanism of electrostatic interaction between biochars and heavy metals. However, the present study did not find peaks shifting from FT-IR results suggesting an adsorption mechanism of cation-π interaction, which may be due to the detection limit.

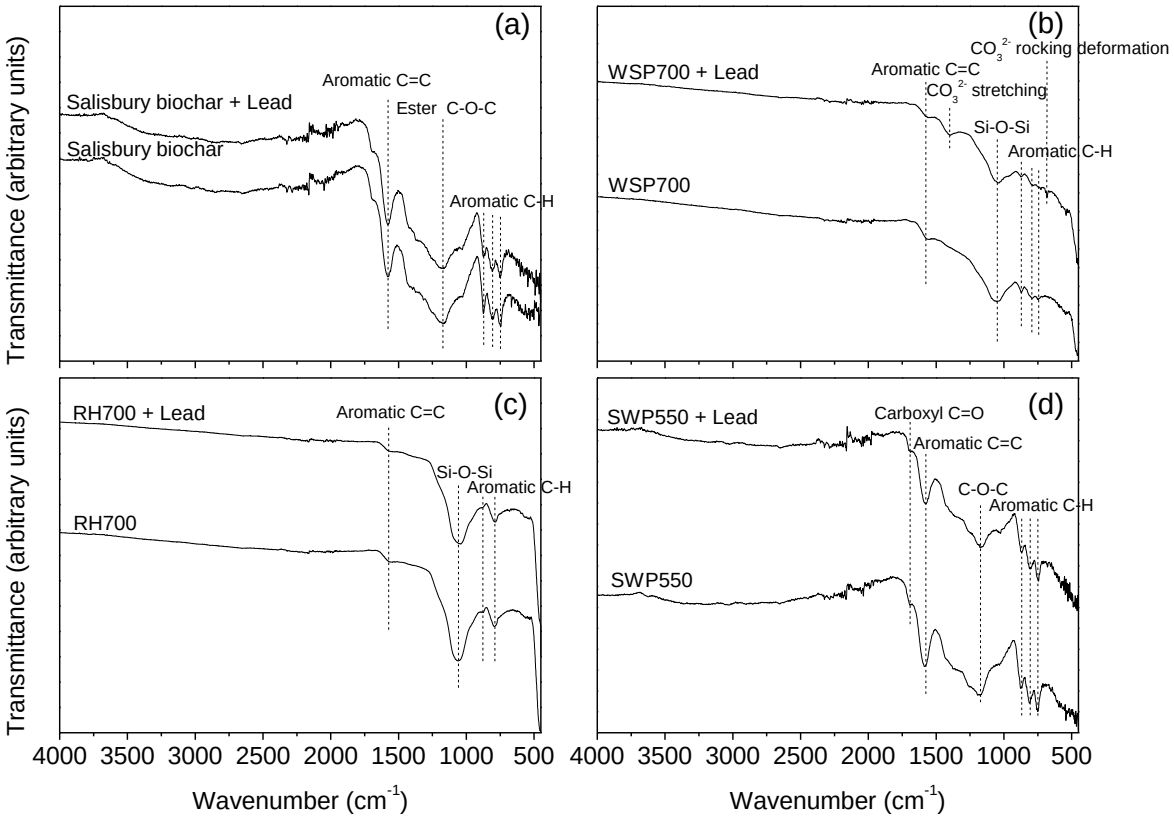

359

360 Fig. 3. FT-IR spectra of biochars before and after Pb^{2+} adsorption (a – Salisbury
361 biochar (SB), b – WSP700, c – RH700, d – SWP550).

362 3.3 TGA results

363 TGA tests were carried out to determine the contents of $Pb_3(CO_3)_2(OH)_2$ or $PbCO_3$
364 on biochars and the results are shown in Fig. 4. $CaCO_3$, lead dichloride ($PbCl_2$) and
365 pyromorphite ($Pb_5(PO_4)_3Cl$), as suggested by XRD results, are stable at this testing
366 temperature range (Chernorukov et al., 2011; Oniyama and Wahlbeck, 1995). Two
367 new peaks on the DTG curve between 223 and 361 °C for SB after Pb^{2+} adsorption
368 (Fig. 4a) were attributed to the thermal decomposition of $PbCO_3$ (Ciomartan et al.,
369 1996), further confirming an adsorption mechanism of surface precipitation. It is of
370 note that various intermediate products (e.g. $PbCO_3 \cdot PbO$ and $PbCO_3 \cdot 2PbO$) may
371 form during the thermal decomposition of $PbCO_3$ to PbO (Sajadi and Alamolhoda,

2006), which can be affected by the experimental conditions and the influence of other substances in the biochar. The two peaks indicate the presence of such intermediate products. However, regardless of the type of the intermediate products, the weight loss between 223 and 361 °C was all attributed to CO_2 loss. The decomposition of $PbCO_3$ to PbO (if only considering the final products) can be expressed as:

$$PbCO_3 \rightarrow PbO + CO_2 \quad \text{Equation 1}$$

According to the TGA results and Equation 1 and taking the biochar sample before Pb^{2+} adsorption as a control, the weight percentage of Pb^{2+} in the form of $PbCO_3$ can be calculated as 3.11%, which is equivalent to 82.24% of the totally adsorbed amount of Pb^{2+} on SB. It was calculated from the sequential extraction results that 85.31% of the totally adsorbed Pb^{2+} on SB was acidic soluble, which coincides well with the TGA results and suggests this acidic soluble fraction was mainly in the form of $PbCO_3$.

Similar to $PbCO_3$, the thermal decomposition of $Pb_3(CO_3)_2(OH)_2$ at the testing temperature range can be separated into several steps. The dehydration process ($Pb_3(CO_3)_2(OH)_2$ to $2PbCO_3 \cdot PbO$) took place between 100 and 200 °C (Sarig and Kahana, 1976), and then the decomposition of $2PbCO_3 \cdot PbO$ to PbO happened between 260 and 370°C, during which a range of intermediate products may present (e.g. $PbCO_3 \cdot PbO$, $4PbCO_3 \cdot 3PbO$ and $PbCO_3 \cdot 2PbO$) (Ciomartan et al., 1996). In this study, the dehydration of $Pb_3(CO_3)_2(OH)_2$ overlapped with the drying process of biochar, which was therefore difficult to be isolated (the big peaks on DTG curves before ~200 °C in Fig. 4). However this will not affect the calculation of the

396 percentage of $Pb_3(CO_3)_2(OH)_2$ on biochar. The new peaks on the DTG curves in the
397 ranges 195-342 °C, 286-339 °C and 288-375 °C for WSP700, RH700 and SWP550
398 after Pb^{2+} adsorption respectively indicate the presence of the intermediate products,
399 further suggesting an adsorption mechanism of surface precipitation. Regardless of
400 the type of the intermediate products, the weight loss ($2PbCO_3 \cdot PbO$ to PbO) was all
401 attributed to CO_2 loss, and therefore the percentage of Pb^{2+} in the form of
402 $Pb_3(CO_3)_2(OH)_2$ on biochar can be calculated based on Equation 1.

403 According to the TGA results and Equation 1, the percentage of Pb^{2+} in the form of
404 $Pb_3(CO_3)_2(OH)_2$ on WSP700, RH700 and SWP550 can be calculated as 1.46%, 0.66%
405 and 0.24% (taking the biochar samples before heavy metal adsorption as control),
406 which are equivalent to 13.00%, 19.19% and 29.70% of the totally adsorbed Pb^{2+}
407 respectively. The sequential extraction results show 75.61% and 85.76% of total
408 adsorbed Pb^{2+} are acidic soluble for WSP700 and RH700 respectively. Therefore,
409 according to the TGA and sequential extraction results, the precipitated Pb^{2+}
410 quantified by TGA only accounted for part of the acidic soluble Pb^{2+} adsorbed on the
411 biochars. There are other mechanisms contributing to the acidic soluble Pb^{2+}
412 adsorbed on the biochars, which may include cation-π interactions.

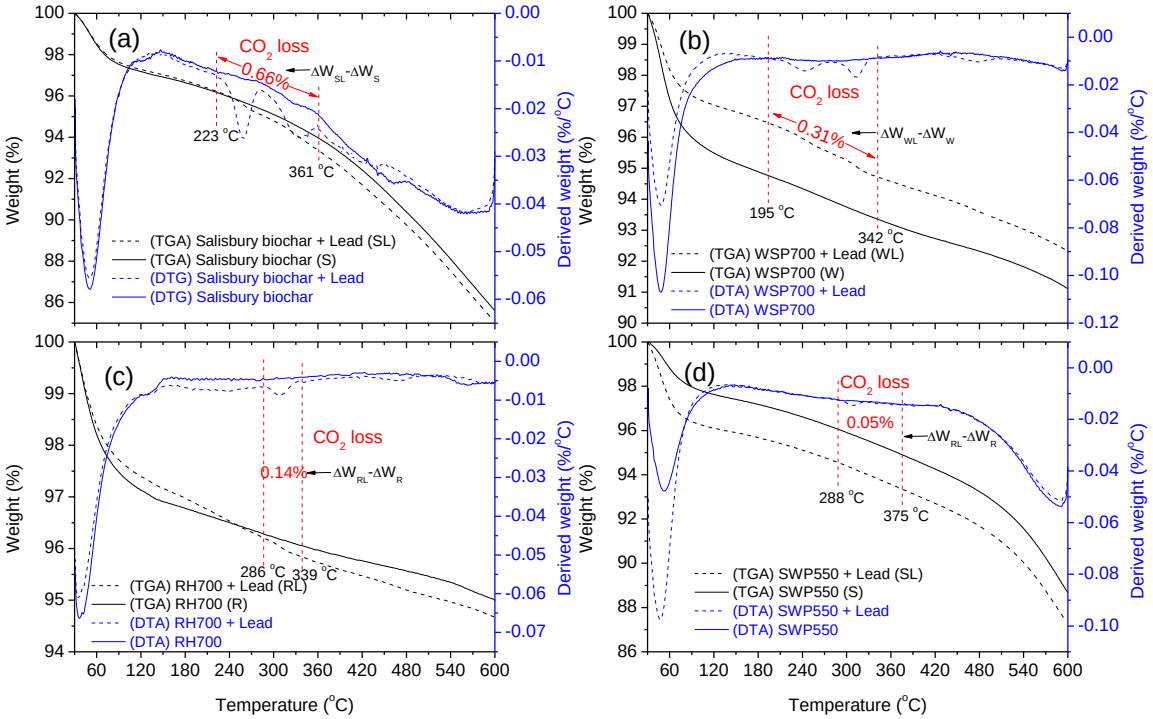

413

414 Fig. 4. TGA and DTG curves of biochars before and after Pb^{2+} adsorption (a –

415 Salisbury biochar (SB), b – WSP700, c – RH700, d – SWP550).

416 3.4 SEM and EDX results

417 The SEM images and EDX results of biochar are shown in Fig. 5, Fig. 6, S2, S3, S4,

418 S5 and S6. Pb^{2+} was observed on the surface of SB (Fig. 5 and S4). This Pb^{2+} may

419 come from Pb^{2+} precipitates, as suggested by XRD, FT-IR and TGA results. The

420 presence of Al^{3+} also suggests it may have exchanged with Al^{3+} on biochar. EDX

421 plots for WSP700 showed the presence of Pb^{2+} both perpendicular and parallel to

422 fibre direction (Fig. S5). Clear solid particles can be seen in plots 1, 3 and 5 (Fig. 6

423 and S5), suggesting the formation of Pb^{2+} precipitates as suggested by XRD and

424 TGA results. Pb^{2+} was also observed on RH700 (Fig. S3 and S6), which may either

425 come from Pb^{2+} precipitates or through cation exchange with K^{+} or Ca^{2+}. The EDX

426 results for SWP550 did not show Pb^{2+} (Fig. S2), which was likely due to the relatively

427 low concentration of Pb^{2+} on SWP550.

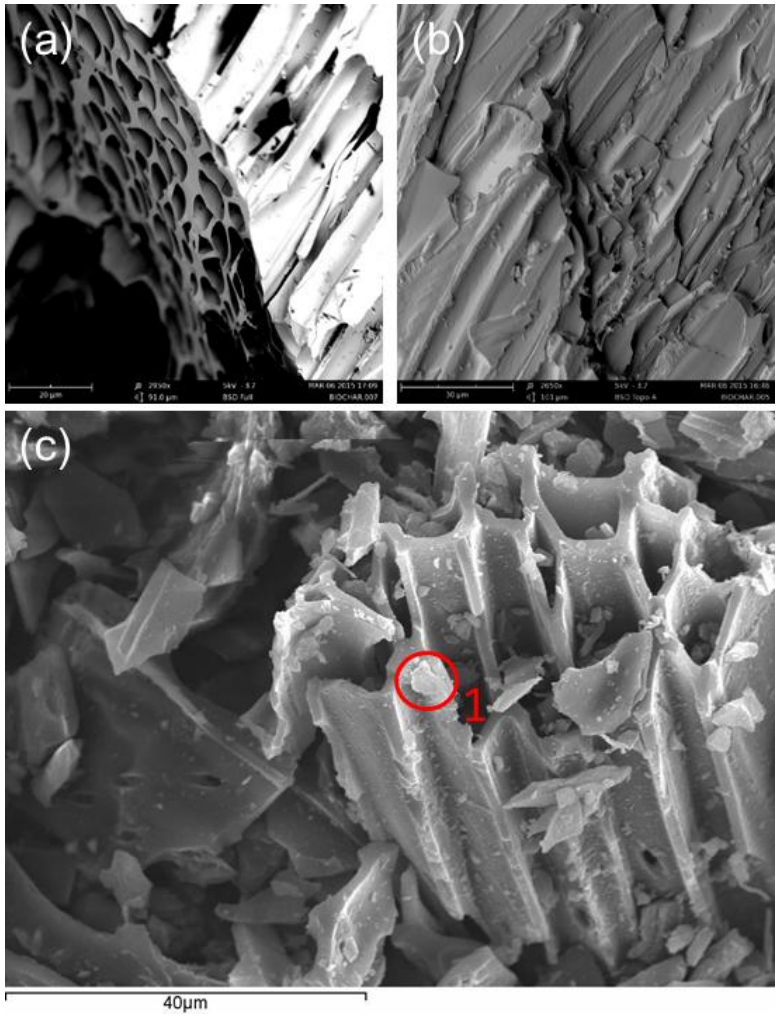

Fig. 5. SEM/EDX images of SB before and after Pb^{2+} adsorption (a – perpendicular to fibre direction before adsorption (Shen et al., 2015), b – parallel to fibre direction before adsorption, c – perpendicular to fibre direction after adsorption. The spectrum for the EDX plot (red circle) is shown in Fig. S4).

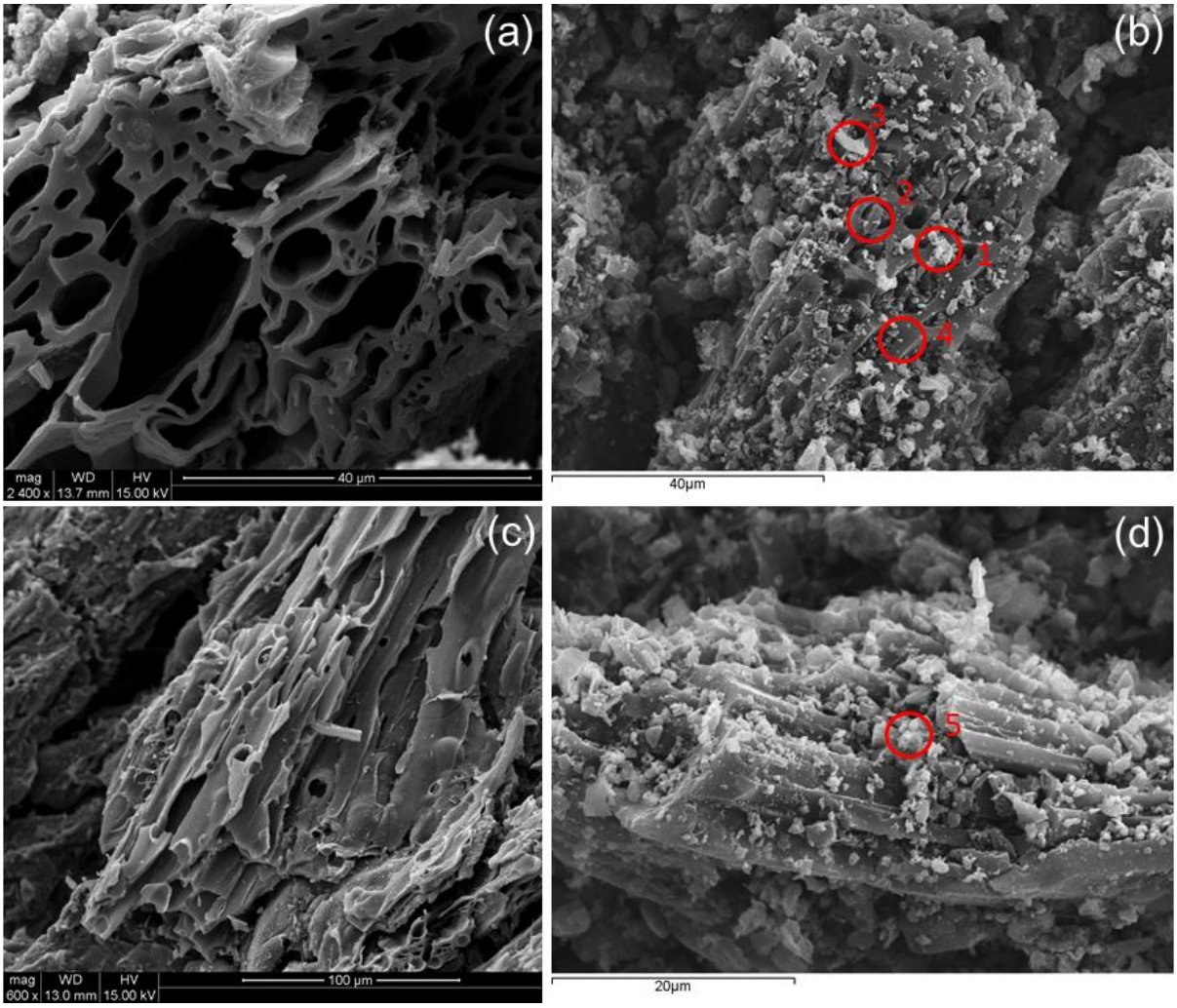

Fig. 6. SEM/EDX images of WSP700 before and after Pb^{2+} adsorption (a – perpendicular to fibre direction before adsorption (Shen et al., 2017a), b – perpendicular to fibre direction after adsorption, c – parallel to fibre direction before adsorption, d – parallel to fibre direction after adsorption. The spectrums for the EDX plots (red circles) are shown in Fig. S5).

3.5 Discussion

SB was previously applied to a field contaminated site (sandy soil) (Shen et al., 2016a) and an artificially contaminated clay soil (kaolin) in laboratory (Shen et al., 2016b). In the field site, it effectively immobilised Ni^{2+}, Zn^{2+} and Pb^{2+} (data for Pb^{2+} not shown) during a three-year study through increasing their non-bioavailable

444 (residual) fraction, while it did not show a significant influence on the mobility or
445 speciation of Pb^{2+} in the kaolin during a 28-day study. It was suggested that the
446 insignificant effect in kaolin was due to the failure for SB to competitively adsorb Pb^{2+}
447 in the acidic environment (pH 4.54-4.92) (Shen et al., 2016b). The present study
448 coincides with that previous study and further confirms that the main mechanism for
449 Pb^{2+} adsorption on SB was through precipitation to $PbCO_3$, and therefore it was
450 difficult for SB to precipitate Pb^{2+} and alter its speciation in the kaolin under such an
451 acidic environment. However, according to the findings from the present study, and
452 considering the soil pH (7.9-8.1) of the field site soil (Shen et al., 2016a), the
453 immobilisation mechanism of Pb^{2+} would likely be the formation of acidic soluble
454 precipitates on the biochar surface representing a potentially bioavailable fraction in
455 the site soil under field conditions. This finding conflicts with the findings from the
456 previous study that the addition of SB increased the non-bioavailable (residual)
457 fraction of heavy metals (Ni^{2+}, Zn^{2+} and Pb^{2+}) on site (Shen et al., 2016a). Previous
458 studies have observed that biochar immobilised heavy metals (Cu^{2+}, Pb^{2+} or Cd^{2+})
459 via conversion to different fractions (e.g. acidic soluble fraction (Ahmad et al., 2016),
460 reducible and oxidisable fractions (Jiang et al., 2012) and residual fraction (Ahmad et
461 al., 2014)) in soils. However these studies did not investigate the speciation of heavy
462 metals after being adsorbed by biochar in aqueous solutions. Therefore the
463 comparison between heavy metal speciation under the two environments (water and
464 soil) cannot be made with those studies. Therefore no references can be found to
465 give hints to the explanation of the conflicting findings regarding the immobilisation
466 mechanism between this study and the site study. It may be due to the alkaline soil
467 aiding biochar's adsorption for heavy metals through precipitation to stable minerals;

468 or biochar strengthening the bonding of heavy metals (i.e. increasing the residual
469 fraction) to soils.

470 Previous studies found that pH and CEC can be good indicators for the adsorption
471 capacities of heavy metals (Cu^{2+}, Ni^{2+} and Pb^{2+}) on the standard biochars, with
472 higher pH and CEC resulting in higher adsorption capacities, which were attributed
473 to the formation of alkaline minerals and an accompanied aromaticity during biochar
474 production (Dodson, 2011). This study confirms that the acidic soluble fraction of
475 Pb^{2+} is the largest fraction on WSP700 and RH700, suggesting adsorption
476 mechanisms of surface precipitation and/or cation-π interaction, which is in line with
477 previous analysis that alkaline minerals and/or accompanied aromaticity controlled
478 the adsorption of heavy metals on the standard biochars (Shen et al., 2017a).
479 Although the CEC value predicts the adsorption capacities of heavy metals on the
480 standard biochars well, it was suggested that this was only due to the fact that CEC
481 value can be an indicator for the occurrence of alkaline mineral contents (Shen et al.,
482 2017a). Cation exchange itself may not be the controlling mechanism in heavy metal
483 adsorption for the standard biochars (Shen et al., 2017a). This study observed that
484 cation exchange made a very small contribution to the adsorption of Pb^{2+} on
485 WSP700 and RH700, confirming that cation exchange played an insignificant role in
486 Pb^{2+} adsorption on the standard biochars and CEC was only an indicator of alkaline
487 mineral contents.

488 It is of note that these experiments are based on the fact that all four biochars
489 reached their maximum adsorption capacities and all of the implications from the
490 results of this study should be based on this assumption. Practical conditions of Pb^{2+}
491 concentrations in soil and water may vary and therefore the applied biochars may
492 not reach their maximum adsorption capacities. The adsorption of Pb^{2+} onto biochar

493 will start with higher energy bindings to lower ones (Shen et al., 2016a). Therefore,
494 the speciation of Pb^{2+} adsorbed on biochar can be easily predicted according to the
495 present sequential extraction results when biochar did not reach their maximum
496 adsorption capacities.

497 4 Conclusions

498 This study quantified different speciation of Pb^{2+} on SB, WSP700 and RH700. The
499 majority of Pb^{2+} was adsorbed on biochar as an acidic soluble fraction, which
500 represents a potentially bioavailable fraction if applied in soil. Within the acidic
501 soluble fraction, the percentage of Pb^{2+} adsorbed through precipitation to $PbCO_3$ on
502 SB and $Pb_3(CO_3)_2(OH)_2$ on WSP700 and RH700 was quantified. Therefore the long-
503 term stability of this fraction under field conditions can be estimated based on the
504 solubility of these precipitates, and the site conditions if these biochars were applied
505 to field contaminated land. It is also possible to model the long-term performance of
506 biochar for soil remediation if the adsorption mechanisms can be quantified and
507 other environmental parameters can be obtained. The pH of field soil may vary due
508 to acidic rainfall, and plant root and microbial activities. Other cations in the soil
509 environment may also compete against Pb^{2+} for precipitation on biochar's surface.
510 Therefore, the estimation and modelling of the long-term performance of biochar in
511 field conditions should carefully consider the various influencing factors. Based on
512 the evidence found from this study, the properties of biochar may be altered by
513 controlling the production process so as to specify the most suitable biochars for a
514 specific engineering usage, however the linkage between biochar field performance
515 and laboratory test results needs careful verification before large-scale application.

516 Acknowledgements

Special thanks go to Dr. Kai Gu from Nanjing University, China, who kindly offered the TGA tests for this study. The standard biochars were obtained from the UK Biochar Research Centre (UKBRC) at the University of Edinburgh. The authors would like to thank Dr. Ondrej Masek from the UKBRC for his kind help in preparing and delivering the biochar samples. Special thanks also go to Dr. Zhen Li from the College of Resources and Environmental Sciences, Nanjing Agricultural University, China, who conducted the SEM tests for the biochars used in this study. The authors would like to thank Mr. Bin Zhao for conducting the elementary and ash analyses for Salisbury biochar. The first author would like to thank the Killam Trusts from Canada for kindly providing the Izaak Walton Killam Memorial Postdoctoral Fellowship.

References

Ahmad, M., Lee, S.S., Lim, J.E., Lee, S.E., Cho, J.S., Moon, D.H., Hashimoto, Y., Ok, Y.S., 2014. Speciation and phytoavailability of lead and antimony in a small arms range soil amended with mussel shell, cow bone and biochar: EXAFS spectroscopy and chemical extractions. Chemosphere 95, 433–441. doi:10.1016/j.chemosphere.2013.09.077

Ahmad, M., Ok, Y.S., Kim, B.-Y., Ahn, J.-H., Lee, Y.H., Zhang, M., Moon, D.H., Al-Wabel, M.I., Lee, S.S., 2016. Impact of soybean stover- and pine needle-derived biochars on Pb and As mobility, microbial community, and carbon stability in a contaminated agricultural soil. J. Environ. Manage. 166, 131–139. doi:10.1016/j.jenvman.2015.10.006

Alhashimi, H.A., Aktas, C.B., 2017. Life cycle environmental and economic performance of biochar compared with activated carbon: A meta-analysis. Resour. Conserv. Recycl. 118, 13–26. doi:10.1016/j.resconrec.2016.11.016

Beesley, L., Moreno-Jiménez, E., Gomez-Eyles, J.L., Harris, E., Robinson, B., Sizmur, T., 2011. A review of biochars' potential role in the remediation, revegetation and restoration of contaminated soils. Environ. Pollut. 159, 3269–82. doi:10.1016/j.envpol.2011.07.023

Bian, R., Joseph, S., Cui, L., Pan, G., Li, L., Liu, X., Zhang, A., Rutlidge, H., Wong, S., Chia, C., Marjo, C., Gong, B., Munroe, P., Donne, S., 2014. A three-year experiment confirms continuous immobilization of cadmium and lead in contaminated paddy field with biochar amendment. J. Hazard. Mater. 272, 121–8. doi:10.1016/j.jhazmat.2014.03.017

Cao, X., Ma, L., Gao, B., Harris, W., 2009. Dairy-manure derived biochar effectively sorbs lead and atrazine. Environ. Sci. Technol. 43, 3285–3291. doi:10.1021/es803092k

Cheng, Q., Huang, Q., Khan, S., Liu, Y., Liao, Z., Li, G., Ok, Y.S., 2016. Adsorption of Cd by peanut husks and peanut husk biochar from aqueous solutions. Ecol.

555 Eng. 87, 240–245. doi:http://dx.doi.org/10.1016/j.ecoleng.2015.11.045
556 Chernorukov, N.G., Knyazev, a. V., Bulanov, E.N., 2011. Phase transitions and
557 thermal expansion of apatite-structured compounds. Inorg. Mater. 47, 172–177.
558 doi:10.1134/S002016851101002X
559 Choy, K.K.H., McKay, G., 2005. Sorption of cadmium, copper, and zinc ions onto
560 bone char using Crank diffusion model. Chemosphere 60, 1141–1150.
561 doi:10.1016/j.chemosphere.2004.12.041
562 Ciomartan, D.A., Clark, R.J.H., Mcdonald, L.J., Odlyha, M., 1996. Studies on the
563 thermal decomposition of basic lead(II) carbonate by Fourier- transform Raman
564 spectroscopy, X-ray diffraction and thermal analysis. J. Chem. Soc., Dalton
565 Trans. 1, 3639–3645.
566 Cui, X., Fang, S., Yao, Y., Li, T., Ni, Q., Yang, X., He, Z., 2016a. Science of the Total
567 Environment Potential mechanisms of cadmium removal from aqueous solution
568 by Canna indica derived biochar. Sci. Total Environ. 562, 517–525.
569 doi:10.1016/j.scitotenv.2016.03.248
570 Cui, X., Hao, H., Zhang, C., He, Z., Yang, X., 2016b. Capacity and mechanisms of
571 ammonium and cadmium sorption on different wetland-plant derived biochars.
572 Sci. Total Environ. 539, 566–575. doi:10.1016/j.scitotenv.2015.09.022
573 DeMessie, B., Sahle-Demessie, E., Sorial, G.A., 2015. Cleaning Water
574 Contaminated With Heavy Metal Ions Using Pyrolyzed Biochar Adsorbents. Sep.
575 Sci. Technol. 6395, 150707112535009. doi:10.1080/01496395.2015.1064134
576 Ding, Y., Liu, Y., Liu, S., Li, Z., Tan, X., Huang, X., Zeng, G., Zhou, Y., Zheng, B.,
577 Cai, X., 2016. Competitive removal of Cd(ii) and Pb(ii) by biochars produced
578 from water hyacinths: performance and mechanism. RSC Adv. 6, 5223–5232.
579 doi:10.1039/C5RA26248H
580 Dodson, J., 2011. Wheat straw ash and its use as a silica source. PhD thesis.
581 University of York.
582 Fristak, V., Pipiska, M., Lesny, J., Soja, G., Friesl-Hanl, W., Packova, a, 2015.
583 Utilization of biochar sorbents for Cd(2)(+), Zn(2)(+), and Cu(2)(+) ions
584 separation from aqueous solutions: comparative study. Env. Monit Assess 187,
585 4093. doi:10.1007/s10661-014-4093-y
586 Haizhou, L.I.U., Korshin, G. V., Ferguson, J.F., 2008. Investigation of the kinetics
587 and mechanisms of the oxidation of cerussite and hydrocerussite by chlorine.
588 Environ. Sci. Technol. 42, 3241–3247. doi:10.1021/es7024406
589 Inyang, M., Gao, B., Ding, W., Pullammanappallil, P., Zimmerman, A.R., Cao, X.,
590 2011. Enhanced Lead Sorption by Biochar Derived from Anaerobically Digested
591 Sugarcane Bagasse. Sep. Sci. Technol. 46, 1950–1956.
592 doi:10.1080/01496395.2011.584604
593 Inyang, M.I., Gao, B., Yao, Y., Xue, Y., Zimmerman, A., Mosa, A., Pullammanappallil,
594 P., Ok, Y.S., Cao, X., 2015. A Review of Biochar as a Low-Cost Adsorbent for
595 Aqueous Heavy Metal Removal. Crit. Rev. Environ. Sci. Technol. 00–00.
596 doi:10.1080/10643389.2015.1096880
597 Jahirul, M.I., Rasul, M.G., Chowdhury, A.A., Ashwath, N., 2012. Biofuels production
598 through biomass pyrolysis- A technological review. Energies 5, 4952–5001.
599 doi:10.3390/en5124952
600 Jiang, J., Xu, R.K., Jiang, T.Y., Li, Z., 2012. Immobilization of Cu(II), Pb(II) and Cd(II)
601 by the addition of rice straw derived biochar to a simulated polluted Ultisol. J.
602 Hazard. Mater. 229–230, 145–150. doi:10.1016/j.jhazmat.2012.05.086
603 Keiluweit, M., Kleber, M., 2009. Molecular-level interactions in soils and sediments:
604 The role of aromatic π-systems. Environ. Sci. Technol. 43, 3421–3429.

605 doi:10.1021/es8033044
606 Keiluweit, M., Nico, P.S., Johnson, M., Kleber, M., 2010. Dynamic molecular
607 structure of plant biomass-derived black carbon (biochar). Environ. Sci. Technol.
608 44, 1247–1253. doi:10.1021/es9031419
609 Lehmann, J., 2007. Bio-energy in the black. Front. Ecol. Environ. preprint, 1.
610 doi:10.1890/060133
611 Lehmann, J., Gaunt, J., Rondon, M., 2006. Bio-char sequestration in terrestrial
612 ecosystems - A review. Mitig. Adapt. Strateg. Glob. Chang. 11, 403–427.
613 doi:10.1007/s11027-005-9006-5
614 Lehmann, J., Skjemstad, J., Sohi, S., Carter, J., Barson, M., Falloon, P., Coleman, K.,
615 Woodbury, P., Krull, E., 2008. Australian climate–carbon cycle feedback
616 reduced by soil black carbon. Nat. Geosci. 1, 832–835. doi:10.1038/ngeo358
617 Li, X., Coles, B.J., Ramsey, M.H., Thornton, I., 1995. Sequential extraction of soils
618 for multielement analysis by ICP-AES. CHEMICAL GEOLOGY. 124, 109–123.
619 Li, X.D., Poon, C.S., Sun, H., Lo, I.M., Kirk, D.W., 2001. Heavy metal speciation and
620 leaching behaviors in cement based solidified/stabilized waste materials. J.
621 Hazard. Mater. 82, 215–30.
622 Liu, Z., Zhang, F.S., 2009. Removal of lead from water using biochars prepared from
623 hydrothermal liquefaction of biomass. J. Hazard. Mater. 167, 933–939.
624 doi:10.1016/j.jhazmat.2009.01.085
625 Mohan, D., Pittman, C.U., Bricka, M., Smith, F., Yancey, B., Mohammad, J., Steele,
626 P.H., Alexandre-Franco, M.F., Gómez-Serrano, V., Gong, H., 2007. Sorption of
627 arsenic, cadmium, and lead by chars produced from fast pyrolysis of wood and
628 bark during bio-oil production. J. Colloid Interface Sci. 310, 57–73.
629 doi:10.1016/j.jcis.2007.01.020
630 Oniyama, E., Wahlbeck, P.G., 1995. Application of transpiration theory to TGA data:
631 Calcium carbonate and zinc chloride. Thermochim. Acta 250, 41–53.
632 doi:10.1016/0040-6031(94)01935-A
633 Qian, L., Zhang, W., Yan, J., Han, L., Gao, W., Liu, R., Chen, M., 2016. Bioresource
634 Technology Effective removal of heavy metal by biochar colloids under different
635 pyrolysis temperatures. Bioresour. Technol. 206, 217–224.
636 doi:10.1016/j.biortech.2016.01.065
637 Qiu, Y., Cheng, H., Xu, C., Sheng, G.D., 2008. Surface characteristics of crop-
638 residue-derived black carbon and lead(II) adsorption. Water Res. 42, 567–574.
639 doi:10.1016/j.watres.2007.07.051
640 Rodriguez-Vila, A., Asensio, V., Forj??n, R., Covelo, E.F., 2015. Chemical
641 fractionation of Cu, Ni, Pb and Zn in a mine soil amended with compost and
642 biochar and vegetated with Brassica juncea L. J. Geochemical Explor. 158, 74–
643 81. doi:10.1016/j.gexplo.2015.07.005
644 Sajadi, S.A.A., Alamolhoda, A.A., 2006. Synthesis and properties of lead oxide
645 carbonate. Inorg. Mater. 42, 1099–1103. doi:10.1134/S0020168506100098
646 Sarig, S., Kahana, F., 1976. Thermal decomposition of basic lead carbonate.
647 Thermochim. Acta 14, 263–268. doi:10.1016/0040-6031(76)85003-4
648 Shen, Z., Jin, F., Wang, F., McMillan, O., Al-Tabbaa, A., 2015. Sorption of lead by
649 Salisbury biochar produced from British broadleaf hardwood. Bioresour. Technol.
650 193, 553–556. doi:10.1016/j.biortech.2015.06.111
651 Shen, Z., McMillan, O., Jin, F., Al-Tabbaa, A., 2016a. Salisbury biochar did not affect
652 the mobility or speciation of lead in kaolin in a short-term laboratory study. J.
653 Hazard. Mater. 316, 214–220. doi:10.1016/j.jhazmat.2016.05.042
654 Shen, Z., Som, A.M., Wang, F., Jin, F., McMillan, O., Al-Tabbaa, A., 2016b. Long-

655 term impact of biochar on the immobilisation of nickel (II) and zinc (II) and the
656 revegetation of a contaminated site. Sci. Total Environ. 542, 771–776.
657 doi:10.1016/j.scitotenv.2015.10.057
658 Shen, Z., Zhang, Y., McMillan, O., Jin, F., Al-Tabbaa, A., 2017. Characteristics and
659 mechanisms of nickel adsorption on biochars produced from wheat straw pellets
660 and rice husk. Environ. Sci. Pollut. Res. 1–11. doi:10.1007/s11356-017-8847-2
661 Sizmur, T., Quilliam, R., Puga, A.P., Moreno-Jiménez, E., Beesley, L., Gomez-Eyles,
662 J.L., 2015. Application of Biochar for Soil Remediation 1–40.
663 doi:10.2136/sssaspecpub63.2014.0046.5
664 Sohi, S.P., 2012. Agriculture. Carbon storage with benefits. Science 338, 1034–5.
665 doi:10.1126/science.1225987
666 Tessier, a., Campbell, P.G.C., Bisson, M., 1979. Sequential extraction procedure for
667 the speciation of particulate trace metals. Anal. Chem. 51, 844–851.
668 doi:10.1021/ac50043a017
669 Wang, J., Xiong, Z., Kuzyakov, Y., 2016. Biochar stability in soil: Meta-analysis of
670 decomposition and priming effects. GCB Bioenergy 8, 512–523.
671 doi:10.1111/gcbb.12266
672 Wang, Z., Liu, G., Zheng, H., Li, F., HaoNgo, H., Guo, W., Liu, C., Chen, L., Xing, B.,
673 2014. Investigating the mechanisms of biochar's removal of lead from solution.
674 Bioresour. Technol. doi:10.1016/j.biortech.2014.11.077
675 Xu, X., Cao, X., Zhao, L., 2013. Comparison of rice husk- and dairy manure-derived
676 biochars for simultaneously removing heavy metals from aqueous solutions:
677 Role of mineral components in biochars. Chemosphere 92, 955–961.
678 doi:10.1016/j.chemosphere.2013.03.009
679 Xu, X., Cao, X., Zhao, L., Zhou, H., Luo, Q., 2014. Interaction of organic and
680 inorganic fractions of biochar with Pb(. RSC Adv. 4, 44930–44937.
681 doi:10.1039/C4RA07303G
682 Yang, Y., Wei, Z., Zhang, X., Chen, X., Yue, D., Yin, Q., Xiao, L., Yang, L., 2014.
683 Biochar from Alternanthera philoxeroides could remove Pb(II) efficiently.
684 Bioresour. Technol. 171, 227–232. doi:10.1016/j.biortech.2014.08.015
685 Zhang, Y., Tang, X., Luo, W., 2015. Metal Removal with Two Biochars Made from
686 Municipal Organic Waste: Adsorptive Characterization and Surface
687 Complexation Modeling. Toxicol. Environ. Chem. 2248, 1–30.
688 doi:10.1080/02772248.2015.1030668
689

Supplementary material for on-line publication only

Click here to download Supplementary material for on-line publication only: supporting information.docx